Hindawi
Complexity
Volume 2020, Article ID 5497241, 18 pages
https://doi.org/10.1155/2020/5497241

Research Article

Multisensor-Based Autonomous Grasp Planning for Mobile Manipulator Navigation System with a Novel Soft Gripper

Heng Zhang,[1,2] **Yingbai Hu**,[3] **Jianghua Duan**,[4] **Qing Gao**,[1,2] **Langcheng Huo**,[1,2] **Qiwen Wang**,[1,2] **and Yongquan Chen**[1,2]

[1]*Shenzhen Institute of Artificial Intelligence and Robotics for Society, Shenzhen, China*
[2]*Institute of Robotics and Intelligent Manufacturing, The Chinese University of Hong Kong, Shenzhen, China*
[3]*Department of Informatics, Technical University of Munich, Munich 85748, Germany*
[4]*Guangdong Provincial Key Laboratory of Robotics and Intelligent System, Shenzhen Institutes of Advanced Technology (SIAT), Chinese Academy of Sciences (CAS), Shenzhen 518055, China*

Correspondence should be addressed to Yongquan Chen; yqchen@cuhk.edu.cn

Received 21 June 2020; Revised 25 September 2020; Accepted 18 October 2020; Published 30 October 2020

Academic Editor: Yanan Li

Mobile manipulators are widely used in different fields for transferring and grasping tasks such as in medical assisting devices, industrial production, and hotel services. It is challenging to improve navigation accuracies and grasping success rates in complex environments. In this paper, we develop a multisensor-based mobile grasping system which is configured with a vision system and a novel gripper set in an UR5 manipulator. Additionally, an error term of a cost function based on DWA (dynamic window approach) is proposed to improve the navigation performance of the mobile platform through visual guidance. In the process of mobile grasping, the size and position of the object can be identified by a visual recognition algorithm, and then the finger space and chassis position can be automatically adjusted; thus, the object can be grasped by the UR5 manipulator and gripper. To demonstrate the proposed methods, comparison experiments are also conducted using our developed mobile grasping system. According to the analysis of the experimental results, the motion accuracy of the mobile chassis has been improved significantly, satisfying the requirements of navigation and grasping success rates, as well as achieving a high performance over a wide grasping size range from 1.7 mm to 200 mm.

1. Introduction

The applications of mobile grasping robots are becoming more and more extensive. The application fields include hospitals [1], restaurants [2], supermarkets [3], factories [4], and hotels [5]. In life, people often need to transfer items. Currently, mobile grasping robots can help us grasp, transfer, and place these items. Amazon and Jingdong have held several mobile grasping robot competitions [6], which promoted the development of mobile grasping robots. However, there is still room for optimization of the control algorithm for mobile control and the grasping mechanism in the grasping process. Therefore, in this paper, a study of performance improvement is carried out, focusing on these two aspects. The overall diagram and system diagram of the robot are shown in Figure 1.

In terms of path planning, there are several popular local path planners, such as fractional-order PD (FOPD) controller [7], Timed-Elastic-Band [8], and DWA [9]. These methods help mobile robots run more efficiently to avoid obstacles and reach the destination via a global path. Especially, due to the high efficiency of DWA, it is widely used in ROS Navigation. In terms of the soft grippers, there are a variety of grippers that are suitable for different situations. Wang et al. published many papers on pneumatic soft grippers and introduced soft grippers in several different scenes [10–15]. Hao et al. proposed grasping characteristics under variable effective lengths [16]. Zhong et al. introduced a soft pneumatic dexterous gripper with convertible grading modes [17]. Batsuren and Yu proposed a soft robotic gripper with chambered fingers for performing in-hand

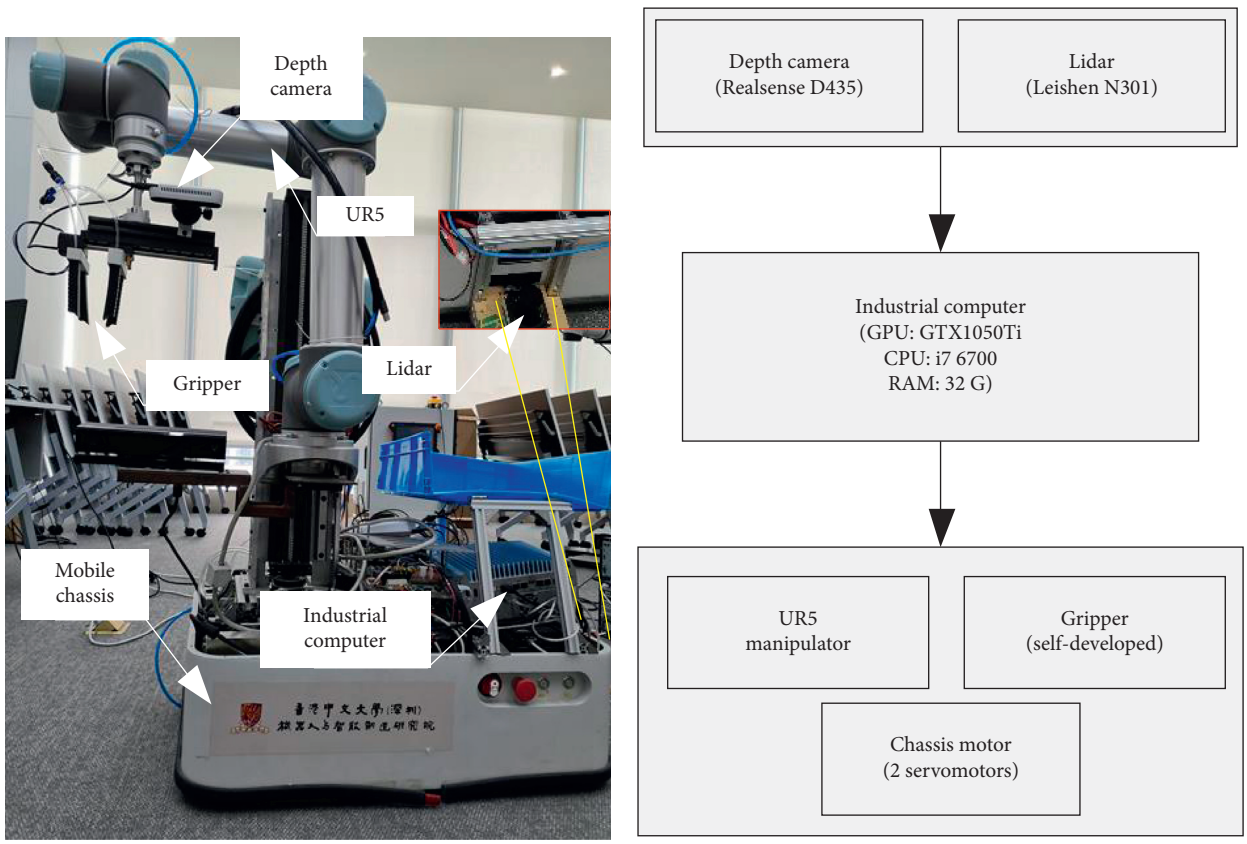

Figure 1: Mobile grasping robot. (a) Photo of the mobile grasping robot. (b) Sensor fusion-based mobile grasping system.

manipulation [18]. Fu and Zhang proposed a soft robot hand with a pin-array structure [19]. In a recent review, Yoon summarized the robust responsive materials, fabrication methods, and applications of soft grippers [20].

However, there are still some shortcomings when the robot is in a complex environment. (1) Because of its fixed parameters, it cannot adapt a complex environment well. (2) It runs poorly in a context with dynamic obstacles. As for the first case, adopt the fuzzy logic controller to change weight parameters to improve its performance [21]. With respect to the second one, predict the motion of obstacles in the future to enhance obstacle avoidance ability [22, 23]. Although there are all kinds of grasping structures, there is still much room to improve the size range of grasping [10, 16–18]. Objects with outer packages or smooth surfaces can be directly grasped by suction cups, but some objects are hard to grasp by suction cups, such as towels without outer packages, knitted gloves, cotton toys, smaller spoons, ear-picks, pens, chopsticks, and toothpicks. To solve these problems, in this study, a pneumatic flexible gripper is designed which can be opened or closed, and the grasping of the above items was performed using this gripper. In order to grasp objects in different positions, a mobile chassis is designed [24]. In order to ensure that the mobile robot runs as close to the global path as possible, an error term of cost function based on DWA is proposed and a comparative trial is carried out between our method and DWA running on ROS [25]. The mobile grasping robotic system designed in this paper uses a combination of the soft gripper, the UR5 manipulator, and the mobile chassis to successfully complete the grasping task.

The innovations and contributions of this paper are as follows: (1) An error term of cost function based on DWA is proposed and a comparative experiment between our method and DWA running on ROS is carried out. (2) A kind of soft gripper for mobile robotic systems with adjustable finger spacing is proposed. The finger structure is optimized, soft grasping is realized, and the range of objects that can be grasped is improved compared with that of the traditional soft gripper [10, 16–18]. (3) The fingers with different shore hardness were analysed by finite element method; then the actual experiment was carried out after printing with 3D printer, and the finger with the largest fingertip force under the same air pressure was selected. (4) The grasping stability coefficient of grasping objects is modelled and the optimal solution is calculated by genetic algorithm. Furthermore, the relationships between the success rate of grasping and grasping stability coefficient, air pressure, and weight are analysed.

The remainder of this paper is arranged as follows. In Section 2, the proposed gripper is introduced. In Section 3, the finite element analysis of a single finger with three kinds of Shore hardness values is carried out. Then, after the fabrication of a single finger with three kinds of Shore

hardness values, the bending angle and fingertip force of the fingers under different air pressures are tested. Additionally, the finger end running track is calculated, and the last finger is selected according to the fingertip force. In Section 4, a new error term of cost function for local path planning is modelled and the grasping model is established. At last, the grasping stability coefficient is calculated. In Section 5, a comparative experiment is carried out to verify our method performance. After the gripper is assembled in the mobile grasping robot, the grasping experiment is carried out, and the results are compared with those of an existing gripper. The paper is concluded in Section 6 with suggestions for future work.

2. The Mobile Grasping System and the Design of the Gripper

2.1. Control of the Mobile Grasping Robotic System. During the process of automatic grasping, when the system receives the grasping command, the mobile chassis first moves to the position where the object is stored, in accordance with the path planning. Then the visual algorithm recognizes the target object to be grasped and sends the corresponding grasping strategy (the grasping strategy includes the chassis position, the grasping path, and the opening size of the grippers). According to the grasping strategy, the system sends the position control command to the microcontroller of the gripper and adjusts the chassis position to a position convenient for grasping. The stepping motor rotates forward or reverses according to the command. At this time, the fingers fixed on the stepper motor remain motionless. The finger fixed on the slider moves away from or near the stepping motor and moves to the designated position according to the number of pulses calculated by the single-chip microcomputer to realize the grasping of objects of different sizes. The UR5 manipulator makes the gripper move to the location of the object, and then the gripper grasps the object. The whole process can realize the grasping of objects of different sizes, as shown in Figure 2.

In terms of the finger spacing control, for example, when grasping bread, the visual algorithm recognizes that the object to be grasped is bread. After analysis, it is found that the optimal grasping size of the gripper is 100 mm. Suppose that the last object grasped is milk, and the opening size of the corresponding gripper is 50 mm. Then, the stepper motor rotates forward, and the fingers fixed on the slider move away from the stepper motor. After sending 5000 pulses, the gripper opens to 100 mm.

2.2. Design Idea of the Gripper. When individuals try to grab large objects, they usually use two hands to clamp the object, as shown in Figure 3. In this paper, according to grabbing habits of individuals, we propose a kind of soft gripper that can simulate human hand grabbing. If this kind of gripper can grab many kinds of goods in daily life, then it will be very helpful for grasping robots.

2.3. Structure Design of Fingers. The finger design structure of Wang et al. [12] is based on the wrinkle shape design idea of the pleated-type morphology of the fluidic elastomer robot. Based on this design structure, many convex points are designed on the cover surface of the finger in this paper. The purpose is to increase the friction with the contact object and improve the reliability of grasping. The design method of the pointed and flat fingertip at the end of the finger uses two opposite fingers to grasp small commodities, such as earpick. A single finger consists of 12 air chambers, each of which is 1.5 mm thick except for the air chambers at both ends. The air chamber width of the designed finger is 5 mm, and the total length of the finger is 88 mm. The single finger section is shown in Figure 4.

Figure 4(a) depicts a chamber, and Figure 4(b) illustrates a cover. The two parts are bonded together to form a pneumatic finger. The section view of the pneumatic finger is shown in Figure 4(c). When inflated to the pneumatic finger, each air chamber will expand like a balloon. Because of the expansion of each air chamber, the air chambers will repel each other, causing the finger to bend. When multiple fingers are combined, the function of grasping objects can be realized.

2.4. Structure Design of the Gripper. To grasp as many kinds of objects as possible, we choose a linear motor. The principle of the linear motor is to use a stepping motor to drive a screw rod to rotate and use the screw rod to drive a slider to slide. The whole gripper is mainly composed of three parts: a linear motor, four soft fingers, and a connecting bracket between the linear motor and soft fingers. Two of the four soft fingers are fixed on the slider, and the other two are fixed on the stepping motor. Furthermore, the sliding of the slider can change the size of the grasping space, and the linear motor of different lengths can be selected according to the different objects to be grasped. To facilitate the experiment, a 200 mm linear motor is selected in this paper. The overall design structure diagram of the gripper is shown in Figure 5.

The two ends of the sider rail of the linear motor are equipped with limit switches, which can prevent the slider from running beyond the limit range. The control of the linear motor is controlled by a single-chip microcomputer (STM32F103C8T6). After the serial port of the single-chip microcomputer receives the instruction of running to a certain target position sent by the industrial computer, the single-chip microcomputer program counts the steps of the stepping motor to make the slider move to the target position. Combined with the advantages of the variable grasping space of the slide, the strategy of grasping objects of various sizes is realized.

3. Finger Performance Evaluation

3.1. Finite Element Analysis. To verify the feasibility of the finger design, finite element mechanical analysis is carried out in ABAQUS (Dassault Systèmes, MA). In the simulation, three kinds of 3D printing rubber-like materials are selected,

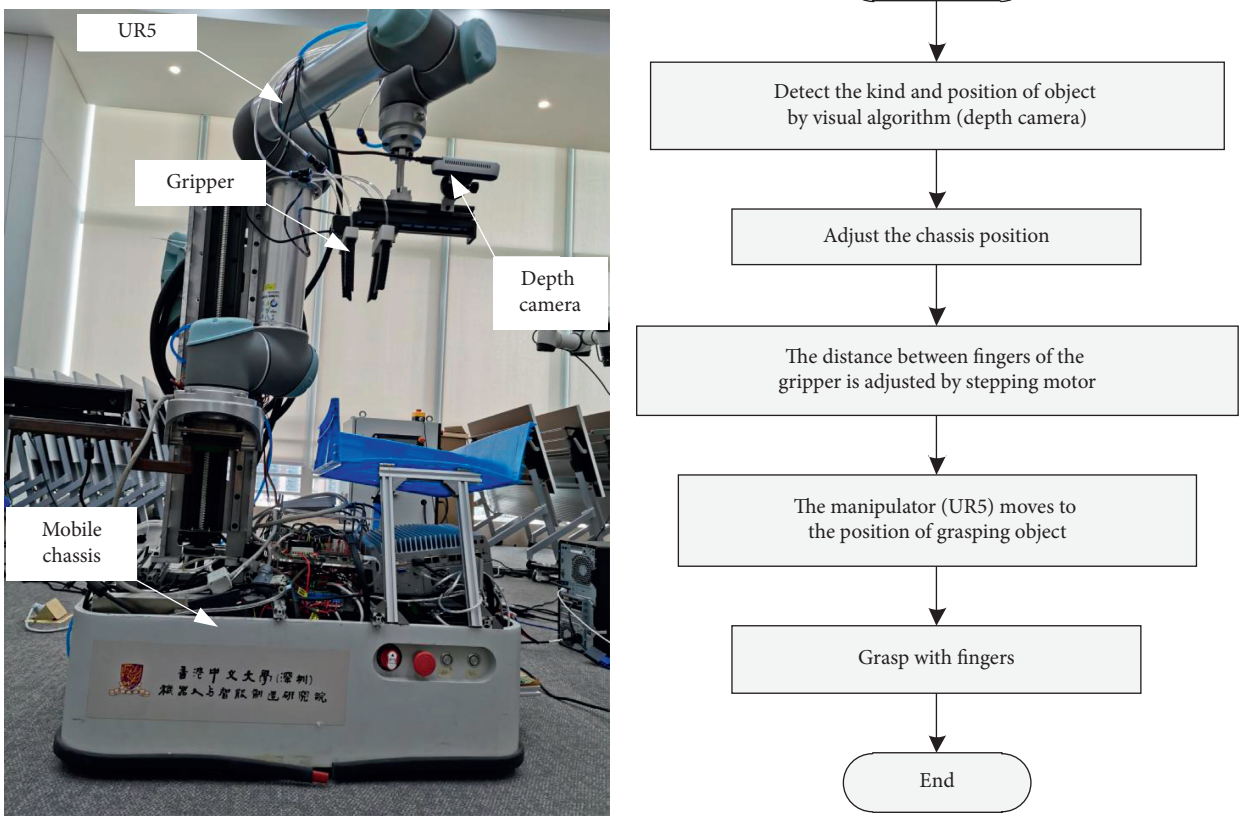

Figure 2: Grasping function of the mobile robot. (a) Mobile grasping robotic system. (b) Robot grasping flow chart.

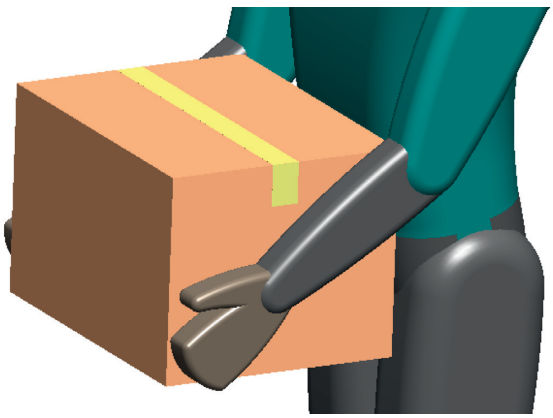

Figure 3: Man grabbing a box.

with Shore hardness values of 30, 50, and 70. The material properties in ABAQUS cannot be directly input into the Shore hardness, and the conversion equation from the Shore hardness to Young's modulus is as follows [26]:

$$E(\text{MPa}) = \frac{0.0981(56 + 7.66s)}{0.137505(254 - 2.54s)}, \quad (1)$$

where s denotes the Shore hardness and E denotes Young's modulus. The calculation results are shown in Table 1.

Because rubber-like materials are usually incompressible, we set Poisson's ratio to 0.49. Set the upper surface of the cover and the part bonded to the chamber as the nontensile fibre cloth material; the elastic module is 6.5 GPa, and Poisson's ratio is 0.2. The contact between the sidewalls of the chamber is set to be friction-free. A tetrahedron is used for mesh, and the mesh size is 2 mm. The finite element analysis is performed after all settings are completed.

The rubber fingers with Shore hardnesses of 30, 50, and 70 were analysed by the finite element method. The corresponding analysis results are shown in Figures 6(a)–6(c).

Under the action of gravity, the fingers will bend to a certain extent, and the smaller the Shore hardness is, the larger the bending angle is. The bending angle α defined in this paper is shown in Figure 6(b). The bending angle curves of the three kinds of Shore hardness fingers under different air pressures are shown in Figure 6(d). From the simulation experiment, it is found that, for fingers with the same Shore hardness, the bending angle is approximately proportional to the air pressure. It can also be seen from Figure 6(d) that the smaller the Shore hardness is, the larger the slope is.

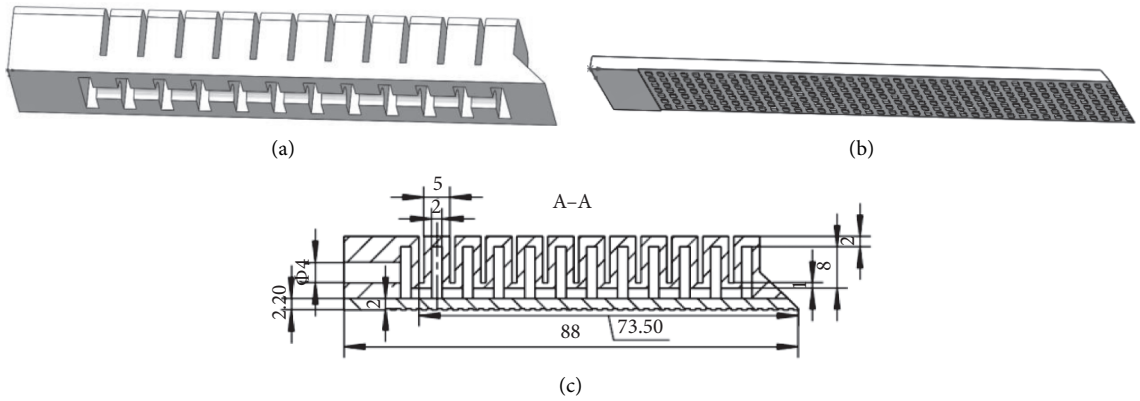

Figure 4: The design process of one finger. (a) The air chamber part of the finger. (b) The cover part of the finger. (c) The section view of the finger.

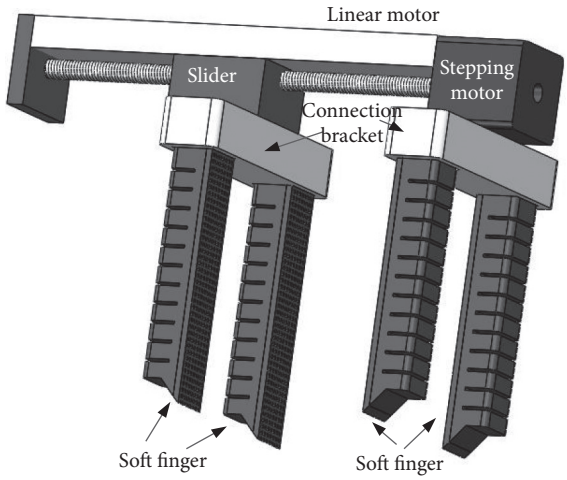

Figure 5: Overall design structure diagram of the gripper.

Table 1: Material properties.

Shore hardness	Young's modulus (MPa)
30	1.1468
50	2.4661
70	5.5445

By using the linear fitting in Origin software, the linear equations of the relationship between the bending angles α [°] of the fingers with Shore hardnesses of 30, 50, and 70 and the air pressure P [kPa] are fitted as equations (2)–(4), respectively:

$$\alpha = 1.87166P + 4.06845, \tag{2}$$

$$\alpha = 0.97143P + 1.67474, \tag{3}$$

$$\alpha = 0.51338P + 1.105. \tag{4}$$

The linear correlation coefficient R and standard deviation S of the finger fitting equation of the three kinds of Shore hardness values are shown in Table 2. The correlation coefficient is a statistical index used to reflect the close relationship between variables. The calculation equation of the linear correlation coefficient R is as follows:

$$R(P, \alpha) = \frac{\mathrm{Cov}(P, \alpha)}{\sqrt{\mathrm{Var}[P]\mathrm{Var}[\alpha]}}, \tag{5}$$

where $\mathrm{Cov}(P, \alpha)$ is the covariance of P and α, $\mathrm{Var}[P]$ is the variance of P, and $\mathrm{Var}[\alpha]$ is the variance of α.

Table 2 and Figure 6(d) show that P is approximately linearly proportional to α. In the simulation, equations (2)–(4) can be used to predict the bending angle of fingers under different air pressures, and the hardness of fingers is 30, 50, and 70, respectively.

3.2. Fabrication of a Single Finger and Experiments. Because of the complex cavity structure of soft grippers, machining is difficult. At present, the commonly used manufacturing processes are shape deposition manufacturing technology (SDM) [27, 28], soft lithography [29, 30], lost-wax casting [31, 32], and 3D printing of composite materials [33]. Because 3D printers have high resolution [10], the performance of each printed finger has better consistency and repeatability. The 3D printer (Objet500 Connex3 system, Stratasys, Minnesota, USA) used in this study can print rubber-like materials with the highest precision of 0.02 mm and a layer thickness of 0.036 mm.

After 3D printing, ERGO5881 glue made in Switzerland is used to tightly stick the cover to the chamber. The air pressure controller uses the active controller PCU-SMN produced by Rochu; its adjustable pressure range is 0 kPa to 120 kPa, and it can also output a nonadjustable negative pressure of −70 kPa. The rubber fingers with Shore hardness values of 30, 50, and 70 are tested under different air pressures. The corresponding experimental results are shown in Figures 7(a)–7(c).

Under the action of gravity, consistent with the conclusion of the simulation results, the lower the Shore hardness is, the greater the bending angle is. The relationships between the bending angle and air pressure for different soft fingers are shown in Figure 7(d). Because the

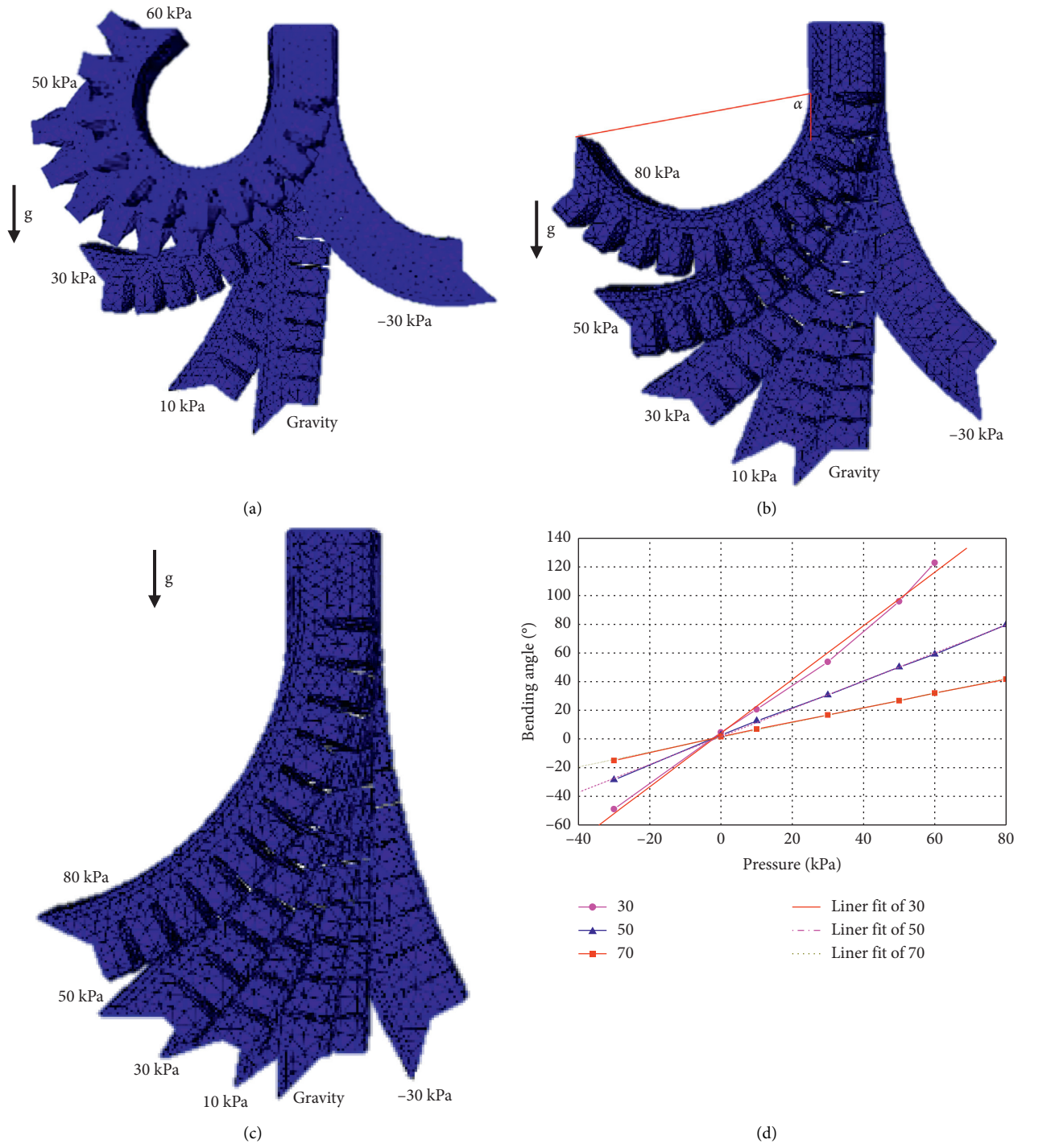

Figure 6: Results of the finite element analysis. (a) The deformation of the fingers with Shore hardness of 30 under different air pressures. (b) The deformation with Shore hardness of 50 under different air pressures. (c) The deformation with Shore hardness of 70 under different air pressures. (d) The relationships between the air pressure and bending angle for different soft fingers.

negative pressure is not adjustable in the experiment, the negative pressure in Figure 7(d) is only −70 kPa. There is a certain difference between the actual experimental and simulation results. This difference may be because the simulation model used in ABAQUS needs to be improved or because of some deviation in the hardness of the 3D printed materials. However, the trend of the simulation results is consistent with the actual results. In the positive pressure part, the bending angle of the fingers with the same Shore hardness is approximately proportional to the air pressure, which is consistent with the conclusion of the simulation. In the actual experiment, the negative pressure is only −70 kPa, and the bending has almost reached the limit at −70 kPa, which does not indicate a difference with

Table 2: Correlation coefficient and standard deviation of the three kinds of finger bending angle fitting.

Shore hardness	R	S
30	0.99742	5.04313
50	0.99972	0.9667
70	0.99968	0.545

the simulation results, so only when the air pressure is greater than 0 kPa are the simulation and experimental results compared.

Using the linear fitting function in Origin software, when the air pressure is greater than 0 kPa, the linear equations of the relationship between the three finger bending angles α [°] with Shore hardness values of 30, 50, and 70 and the air pressure P [kPa] are fitted as equations (6)–(8), respectively:

$$\alpha = 3.13366P + 3.08763, \tag{6}$$

$$\alpha = 2.21799P - 5.29767, \tag{7}$$

$$\alpha = 1.82175P - 4.89558. \tag{8}$$

The correlation coefficient R and standard deviation S of the linear fitting equation of the three kinds of Shore hardness fingers are shown in Table 3.

In practical use, we can roughly predict the degree of curvature of the fingers that correspond to Shore hardness values of 30, 50, and 70 by equations (6)–(8), respectively.

To further understand the performance of fingers, the fingertip force is tested. The type of dynamometer used is SF-50, the measuring range is −50 N to 50 N, and the resolution is 0.01 N. The test diagram of the fingertip force is shown in Figure 8(a). The upper end of the finger is fixed to the bracket, and the contact surface of the fingertip and the dynamometer is fully contacted. Under the action of gravity, the indicator number of the dynamometer is 0 N. With an increase in air pressure, the indicator number of the dynamometer begins to increase gradually. The relationship between the fingertip force and air pressure is shown in Figure 8(b).

Figure 8(b) shows that the fingertip force of the same Shore hardness finger is approximately proportional to the air pressure, while the smaller the Shore hardness is, the greater the fingertip force is. Because of the error of the dynamometer or the error of air pressure adjustment, the curve of fingertip force and air pressure does not completely exhibit a straight line.

Using the linear fitting function in Origin, the equations of the relationship between the fingertip force F [N] and the air pressure P [kPa] with Shore hardnesses of 30, 50, and 70 are fitted as equations (9)–(11), respectively:

$$F = 0.00926P - 0.06067, \tag{9}$$

$$F = 0.00857P - 0.05857, \tag{10}$$

$$F = 0.00825P - 0.0875. \tag{11}$$

The correlation coefficient R and standard deviation S of the finger fitting equation of Shore hardnesses of 30, 50, and 70 are shown in Table 4.

In practical use, the fingertip force under different air pressures can be roughly predicted by equations (9)–(11).

3.3. Analysis of the Fingertip Movement Track. During the process of grasping the object, after the robot moves to the grasping position, the finger moves until it contacts the object [34, 35]. For soft fingers, if the influence of the gravity is ignored before touching the object, then the bending of the fingers caused by air pressure can be regarded as a circular arc, as shown in Figure 9.

After the finger is bent, the arc radius is R, the arc length s is the effective bending length of the finger, l is the chord length, and the centre angle of finger bending is φ. The plane coordinate system is established at the first air chamber of the finger root. The y-axis is tangent to the arc, and the x-axis is through the centre of the circle. According to the geometric relationship, we obtain the following:

$$\begin{aligned} w &= \frac{s}{R}, \\ l &= 2R\sin\left(\frac{w}{2}\right), \\ x &= -l\sin\left(\frac{w}{2}\right), \\ y &= -l\cos\left(\frac{w}{2}\right). \end{aligned} \tag{12}$$

The fingertip movement track of angle φ is drawn from 0 to π, as shown in Figure 10.

4. Navigation and Gripper Grasping Model

4.1. Local Path Planning. To improve the mobile robot running efficiency, we need the mobile robot to run as close to the global path as possible; therefore, an error term of the cost function based on DWA is defined, as seen in Figure 11.

In Figure 11, the green ellipse denotes a global path, and each red cross denotes a discrete point on the global path. The grey-dashed line and blue arc denote optional local paths generated by DWA. Taking the blue local path as an example, H_0, H_1, H_2, H_3 and $H_4 \in H$ denote each red cross of the global path. L_0, L_1, L_2, L_3 and $L_4 \in L$ denote each discrete point of a local path. L_0 denotes the current position of the robot and the first point of a local path. H_0 denotes the point that has the shortest distance from the robot along the global path. e_0 denotes the deviation between L_0 and H_0. e_1, e_2, e_3, and e_4 are the same. The deviation is exaggerated in the figure. Additionally, $|H_0H_1| = |L_0L_1|$. Five points on the local path are chosen to calculate the deviation relative to the counterpart on the global path. Errors e_1 to e_4 are summed as the error term. Thus, our robot can move along the global path better and improve its efficiency.

The error term of the cost function is

$$J_{\text{error}}(L_k, H) = \gamma(e_1 + e_2 + e_3 + e_4). \tag{13}$$

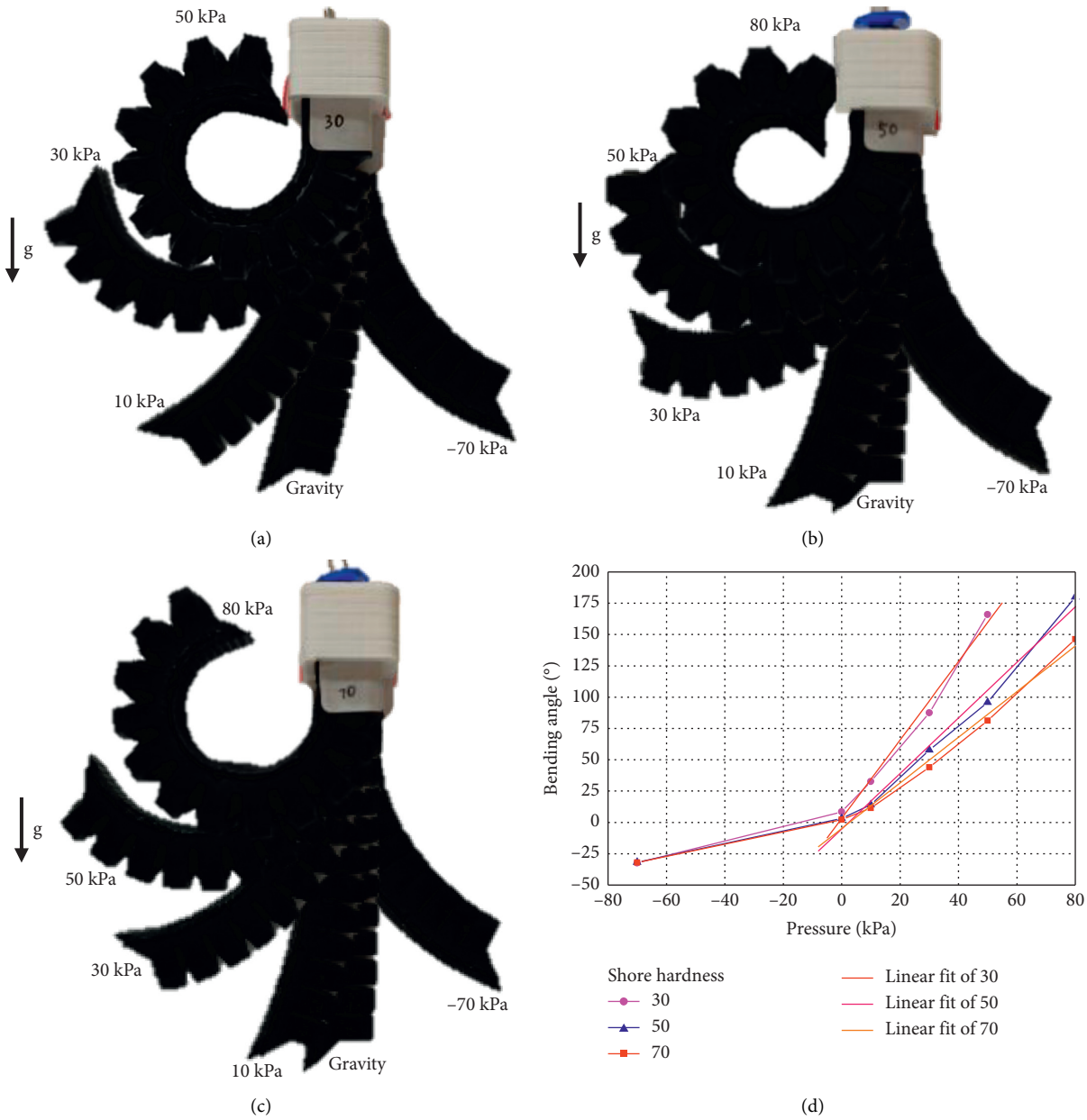

Figure 7: Experimental result. (a) The deformation of the fingers with Shore hardness of 30 under different air pressures. (b) The deformation with Shore hardness of 50 under different air pressures. (c) The deformation with Shore hardness of 70 under different air pressures. (d) The relationships between the air pressure and bending angle for different soft fingers.

L_k indicates the kth optional local path generated by DWA, H indicates the global path, and γ is a weight parameter.

4.2. Grasping Modelling. There are many different evaluation schemes for grasp stability. Ko and Chen [36] proposed an optimal grasping manipulation for multi-fingered robots using semismooth Newton method. Li and Sastry [37] established a generalized external force ellipsoid. The minimum singular value of the grasping matrix G is calculated, and the singular value is used to describe the distance of the position of the contact point from the singular grasping position to quantitatively describe the grasping stability. Xiong and Xiong [38] introduced the grasping stability coefficient w to quantify the grasping stability. This performance index is related to the shape characteristics of the grasping object and the position of the contact point on the surface of the grasping object, that is, the grasping matrix G. The larger the stability coefficient w is, the higher the grasping stability is. w is $0 \le w \le 1$ after normalization, and its expression is as follows:

$$w = \sqrt{\det\left(GG^T\right)}. \tag{14}$$

Table 3: Correlation coefficient and standard deviation of the three kinds of finger bending angle fitting.

Shore hardness	R	S
30	0.99437	9.07033
50	0.99387	9.1398
70	0.99489	6.85057

As shown in Figure 12, the reference coordinate system $\{O\}$ is fixed on the object to be grasped, and the schematic diagram of the contact between the ith finger and the object is shown. The representation r_i is the vector representation of the ith contact point in the reference coordinate system, and $r_i = (x_i \ y_i \ z_i)^T$. $\{C_i\}$ is the contact coordinate system of the ith contact point, whose origin coordinate coincides with the contact point, and the z-axis is along the normal direction of the contact point. Force f_{ci} is the contact force at the ith contact point. The components f_{cix} and f_{ciy} are the tangential components of the contact force, and f_{ciz} is the normal component of the contact force. $f_c = (f_{c1} \ f_{c2} \cdots f_{cm})^T$.

The grasping matrix G can be expressed as follows:

$$G = \begin{pmatrix} I & \cdots & I \\ R_1 & \cdots & R_m \end{pmatrix} \in R^{6\times 3m}, \tag{15}$$

where I is the unit matrix and $I \in R^{3\times 3}$. Ri is

$$R_i = \begin{pmatrix} 0 & -z_i & y_i \\ z_i & 0 & -x_i \\ -y_i & x_i & 0 \end{pmatrix}. \tag{16}$$

The combined external force and the combined external torque acting on the object are called the combined external force spiral F_a as follows:

$$F_a = \begin{pmatrix} F_x & F_y & F_z & M_x & M_y & M_z \end{pmatrix}^T, \tag{17}$$

where $F = \begin{pmatrix} F_x & F_y & F_z \end{pmatrix}^T$ is the combined external force and $M = \begin{pmatrix} M_x & M_y & M_z \end{pmatrix}^T$ is the external moment.

It is assumed that there is friction point contact between the fingers and the object when a multifingered hand grasps the object; that is, the rolling or sliding of the fingers on the object surface is not considered. According to the theory of helix, the contact between fingers and objects can be regarded as a mapping between the force exerted by fingers on the contact point and the resultant helix of a reference point on the object.

$$Gf_c = -F_a. \tag{18}$$

When a manipulator grasps an object, the finger can only "press" the object but not "pull" the object, so the normal component of the contact force exerted by the finger on the object must be positive; that is,

$$-f_{ciz} \le 0, \quad i = 1, \ldots, m. \tag{19}$$

The contact between the finger and object is the friction point contact. To prevent relative sliding between the finger and object, each contact point must meet the friction constraint condition; that is, the contact force f_{ciz} of each contact point must be located in the friction cone (Figure 13). Specifically, the tangential component of the contact force must be less than or equal to the product of the normal component and friction factor μ; that is,

$$\sqrt{f_{cix} + f_{ciy}} - \mu f_{ciz} \le 0. \tag{20}$$

where β is the friction angle and $\beta = \arctan(\mu)$.

Finally, the optimization problem of the grasp point based on the grasp stability index can be summarized as follows:

$$\begin{cases} \min & \longrightarrow -w = \sqrt{\det\left(GG^T\right)} \\ & Gf_c = -F_a - f_{ciz} \le 0 \\ \text{s.t.} & \sqrt{f_{cix} + f_{ciy}} - \mu f_{ciz} \le 0. \end{cases} \tag{21}$$

4.3. Optimal Grasping Position. The end of the gripper designed in this paper is on a plane. To calculate the optimal distribution of the four fingers, the above grasping model is used to calculate the two-dimensional plane. For example, an object is grasped with an elliptical cross section (without losing generality), assuming that the axis length of the ellipse in the x-axis is a and the axis length in the y-axis direction is b. Then, its polar coordinate form can be expressed as follows:

$$\begin{cases} x = a\cos(\theta), \\ y = b\sin(\theta), \end{cases} \tag{22}$$

where θ is the angle between the line between the origin and the point on the ellipse and the x-axis coordinate.

The coordinates of the two-dimensional plane contact point are known; then the grasp matrix G is obtained, and the optimal solution is calculated by the genetic algorithm. After ten groups of experiments, the results of two groups are shown in Figure 14.

Figures 14(a) and 14(b) represent the first group of calculation results, and Figures 14(c) and 14(d) represent the second group of calculation results. In the first and second groups, the ellipse axis lengths in the x-axis direction are 100 mm and 50 mm, respectively. After calculations, it can be seen that the four grasp points are approximately an arithmetic sequence. To facilitate the comparison in the calculation process, a fixed grasp point $\theta = (\pi/4) \approx 0.785$ is set. Then, through the genetic algorithm calculation to 100 generations, it is found that the θ value of the optimal position is approximately the same. In Figure 14, the optimal grasping positions θ are [0.785, −0.77, −2.317, 2.396] and [0.785, −0.783, 2.359, −2.352], respectively. In Figure 14, the grasp stability coefficient w values are 0.99983 and 0.999999, which are close to 1.

In this paper, the distance between two fingers in the unchangeable direction of the designed gripper is 55 mm, and the distance between the two adjacent points in the y-axis direction calculated by two groups of calculation results

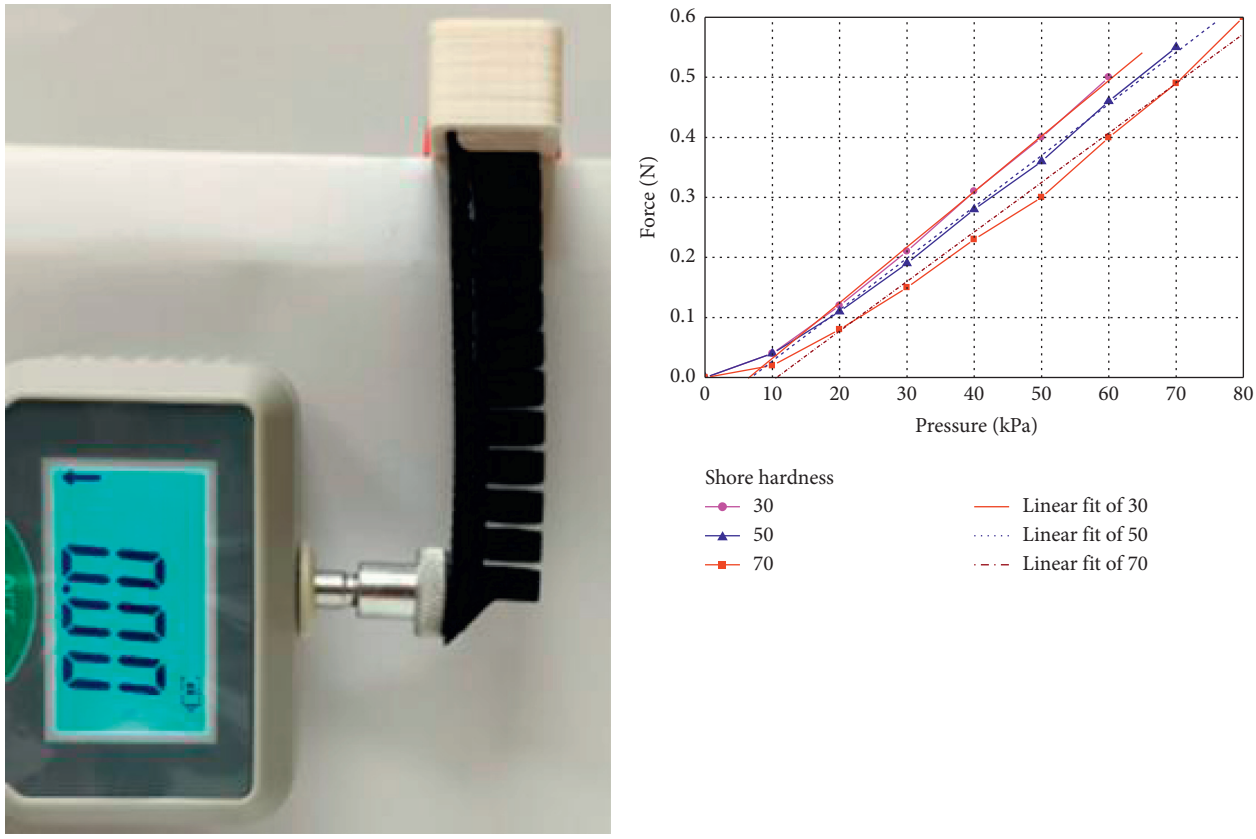

(a) (b)

Figure 8: Fingertip force experiment.

Table 4: Correlation coefficient and standard deviation of the fingertip force fitting.

Shore hardness	R	S
30	0.99944	0.00647
50	0.99889	0.00956
70	0.99596	0.01969

is approximately 56 mm. Therefore, the grasping point of this kind of object can be grasped in the optimal grasping position, and the grasping near the best position can be realized only by adjusting the distance in the x-axis direction. Because the fingers are flexible, during the process of contacting the object surface, they will be in close contact with the object surface under the control of air pressure. In the next structural design, we will add the rotation function of fingers, which may adjust the finger surface to grasp the object.

The gripper designed in this paper cannot reach the optimal grasping point for all objects because the gripper can only change the space between fingers in one direction. However, this does not mean that the gripper cannot successfully grasp the object. When the optimal position cannot be grasped, the value of the grasping stability coefficient w is slightly smaller, and most objects can also be successfully grasped.

5. Experiment and Analysis

5.1. Path Planning Experiment. A comparative experiment is carried out between our method and DWA running on ROS to test the performance. The starting point and goal point remain the same. For the mobile robot motion parameters, see Table 5.

The mobile robot running process can be seen in Figure 15, and the result is shown in Figure 16.

In Figure 16(a), the starting point is (0.1, −0.19), and the goal point is (6.5, −1.45). The blue line denotes a global path generated by the A* algorithm, and the red- and blue-dashed lines denote DWA and our method, respectively. It is clear that our method, which takes an error term into account, yields a better result. In Figure 16(b), the cumulative error is recorded when using different methods. Generally, the error of our method is less than that of DWA. In particular, if the global path is a zigzag pattern, our method will perform better.

5.2. Grasping Experiment. After the experimental analysis of the fingertip force and bending angle of a single finger, it is necessary to further complete the grasping experiment to test the grasping performance. The tracheas of the four fingers are connected together by a quick connector to realize the synchronous bending and grasping function of the four fingers. In the selection of fingers, because fingers with a

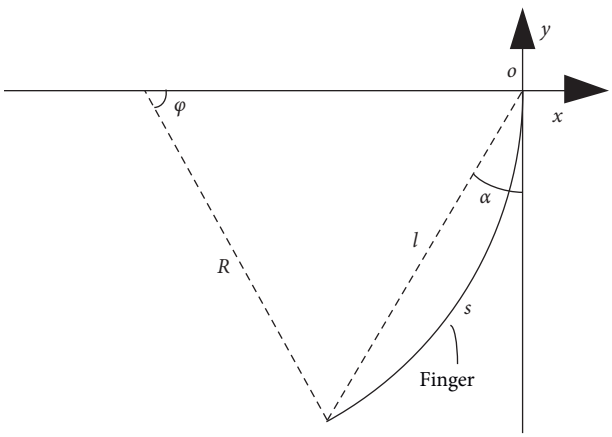

Figure 9: Finger bending analysis.

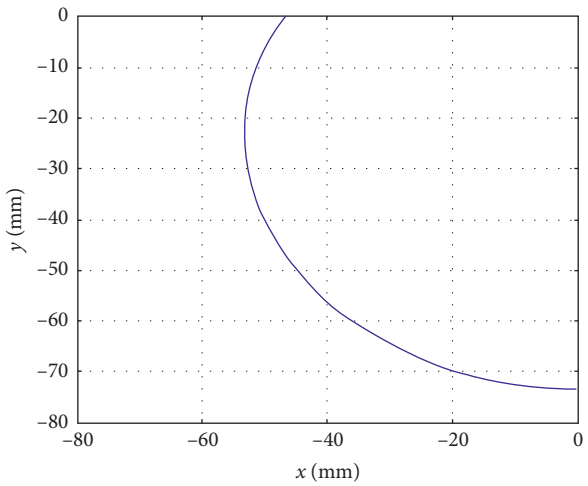

Figure 10: Fingertip trajectory.

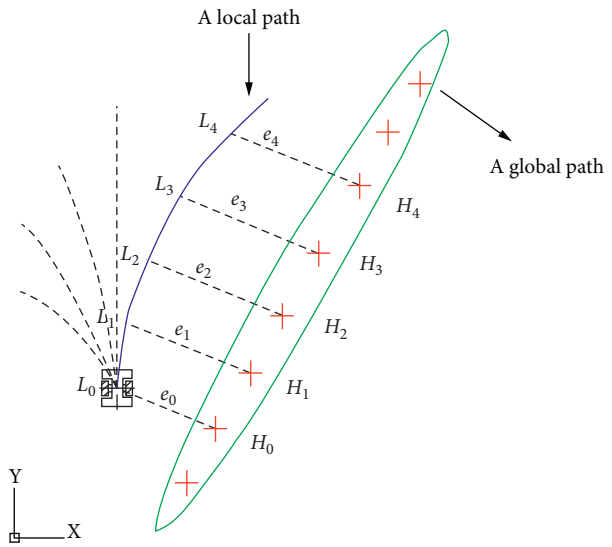

Figure 11: An error term definition.

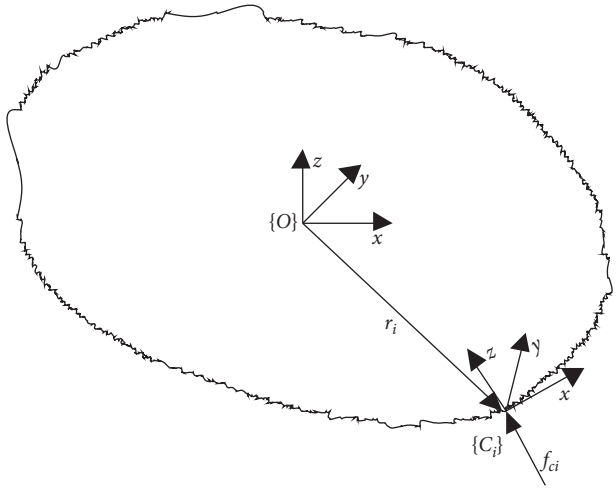

Figure 12: Grasp system model.

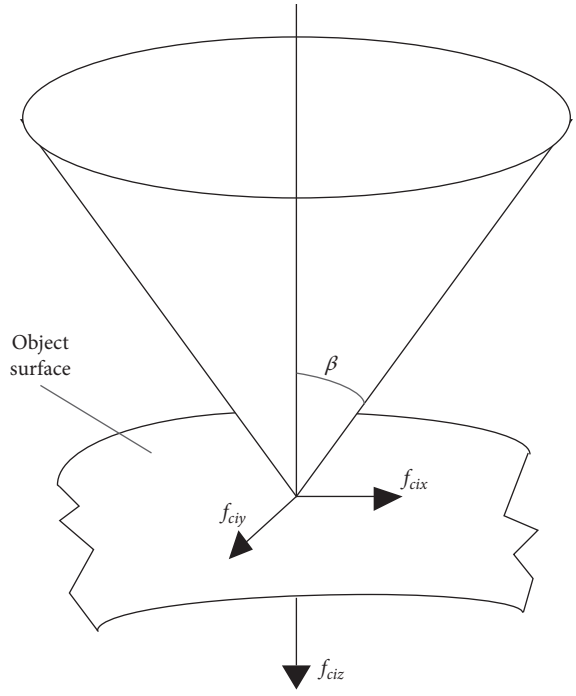

Figure 13: Friction model of the contact point.

Shore hardness of 30 have a greater fingertip force and are softer under the same air pressure, four fingers with a Shore hardness of 30 are selected to form a grasping hand. To verify the grasping performance, 56 kinds of object grasping experiments were conducted, and some grasping results are shown in Figure 17.

Different air pressures are used to grasp different objects; that is, larger air pressures are used for heavier objects, and smaller air pressures are used for lighter objects. The grasping objects include barrelled instant noodles, tissues, a gamepad, steamed cakes, towels, a sponge, an earpick, a toothpick, and even an old business card. During the grasping process, the advantages of the soft gripper are fully embodied with an automatically adjustable finger spacing, which can carry out the grasping of a very small toothpick (1.7 mm in diameter) to a large barrelled instant noodle container (an upper cover with approximately 150 mm diameter). In this experiment, the largest grasp size is a sponge, and its length and width are both 200 mm.

The success rate of the objects in Figure 17 is measured. Each object is grasped ten times and held in the air for more than 10 seconds as a successful attempt. The success rate of grasping is shown in Table 6.

The stability coefficient w is related to the position and shape of the object. Because the finger space of the gripper designed in this paper can only change the finger space in

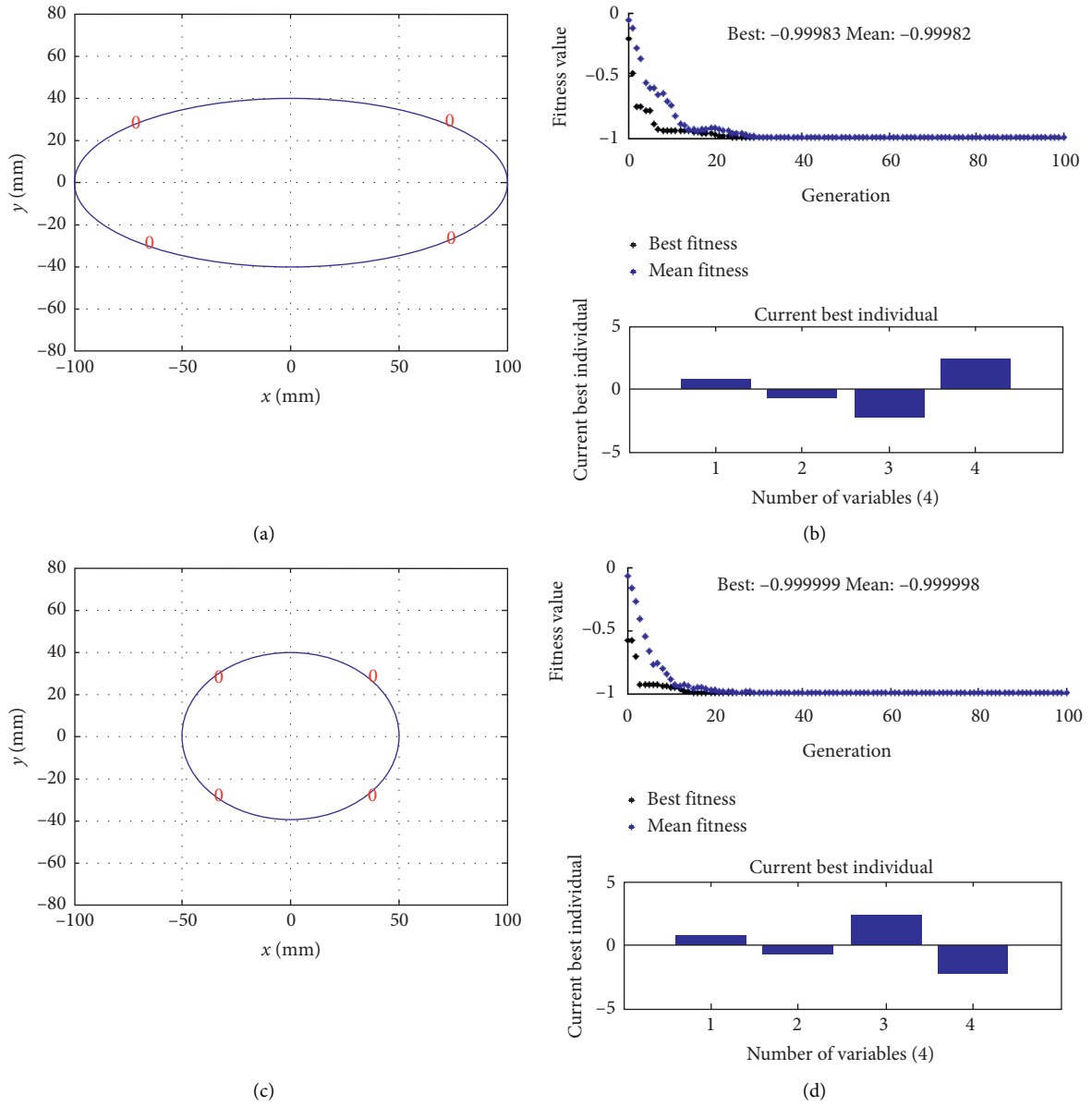

Figure 14: Optimal solution calculation. (a) Ellipse $a = 100$ mm and $b = 40$ mm; the calculated optimal grasp position. (b) Ellipse $a = 100$ mm and $b = 40$ mm; the upper side is the relationship between the fitness value and generation, and the lower side is the value of variable q in the optimal solution. (c) Ellipse $a = 50$ mm and $b = 40$ mm; the calculated optimal grasp position. (d) Ellipse $a = 100$ mm and $b = 40$ mm; the upper side is the relationship between the fitness value and generation, and the lower side is the value of variable q in the optimal solution.

Table 5: Correlation coefficient and standard deviation of the fingertip force fitting.

Parameter name	Value
v_{max}	0.5 m/s
w_{max}	3 rad/s
v'_{max}	0.5 m/s^2
w'_{max}	3 rad/s^2
v_{min}	0 m/s
w_{min}	−3 rad/s
v'_{min}	−2 m/s^2
w'_{min}	−4 rad/s^2

one direction, not all objects can reach the optimal position. Because toothpicks and earpicks are relatively small, they can be grasped with two fingers, which are not comparable to the stability coefficient of four fingers, and the stability coefficient of the two fingers is not calculated. The shape of the gamepad is more complicated, and it is dragged up when grasping, so its stability coefficient is not calculated. According to the analysis of the data, the success rate of grasping is positively related to the grasping stability coefficient and grasping air pressure and negatively related to weight. Therefore, when the stability coefficient decreases,

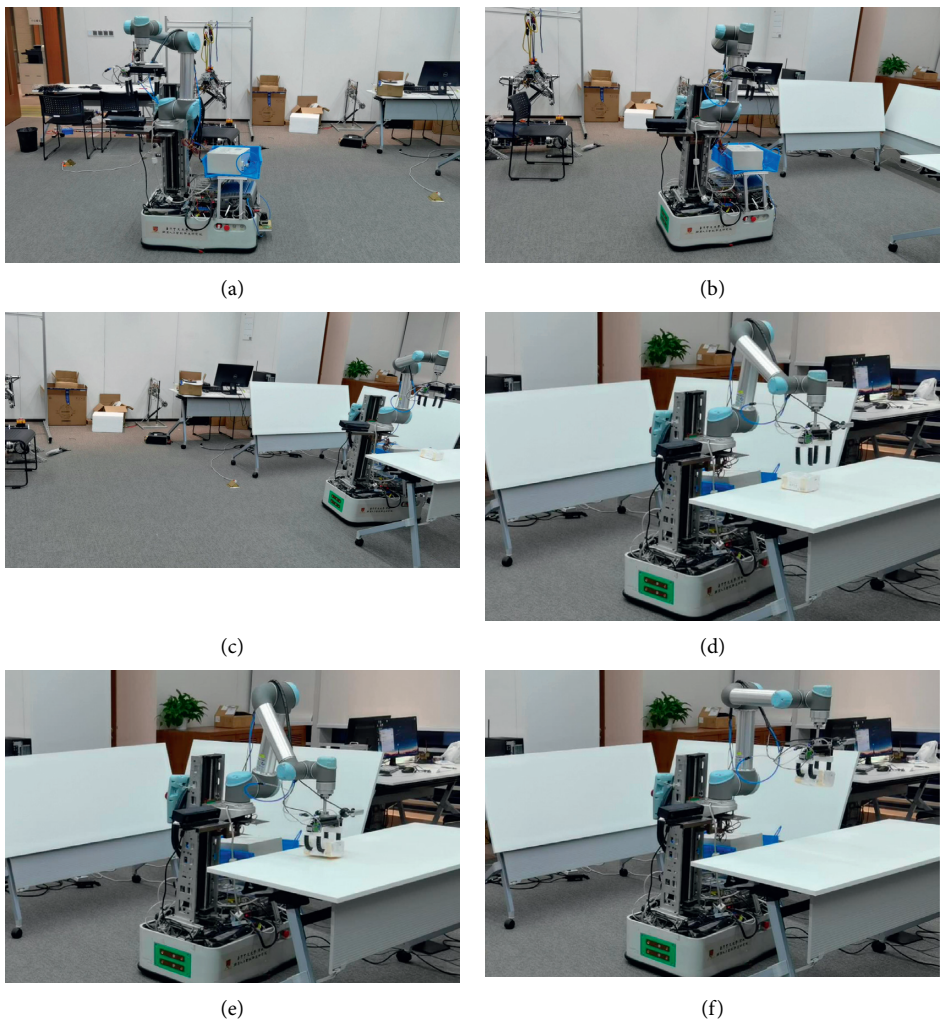

Figure 15: The grasping process of the mobile grasping robot. (a), (b), and (c) move to the destination of the item. (d), (e), and (f) arrive at the destination for grasping.

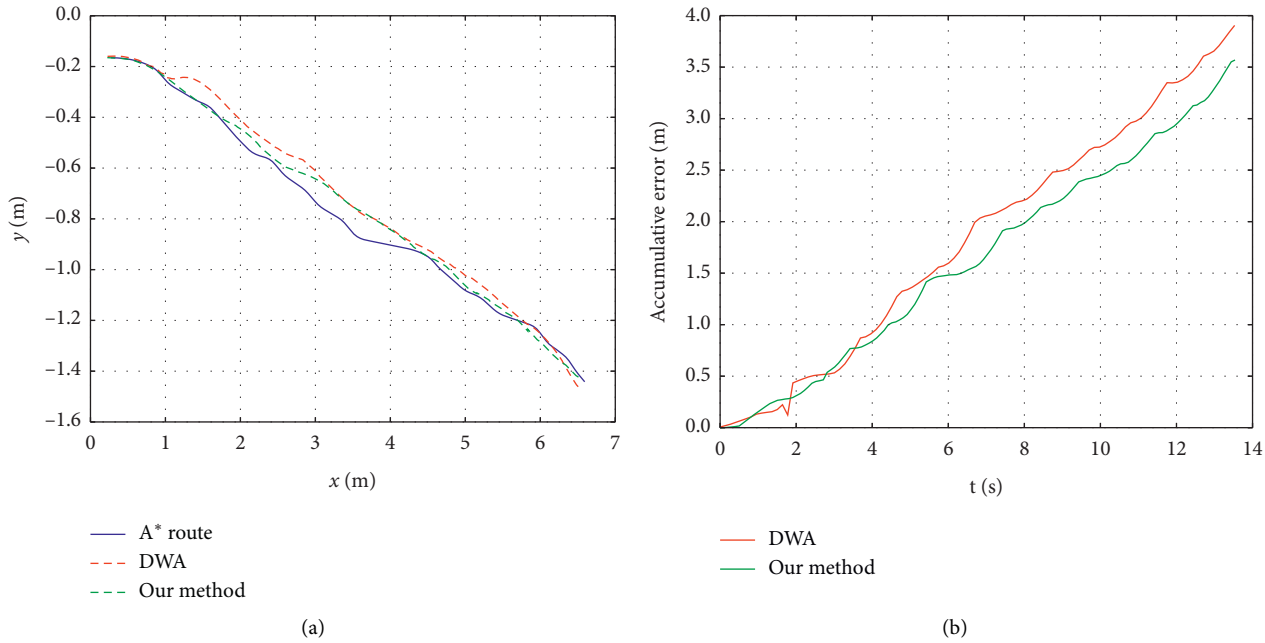

Figure 16: Experiment results. (a) Running trajectory. (b) Cumulative error.

Figure 17: Grasping experiment. (a) Instant noodles. (b) Tissues. (c) Gamepad. (d) Steamed cake. (e) Towel. (f) Sponge. (g) Earpick. (h) Toothpick. (i) Business card.

Table 6: The success rate of grasping.

Object	Size (mm)	Weight (g)	Pressure (kPa)	Success rate (%)	w
Instant noodles	$\varphi 150 \times \varphi 120 \times 110$	191	60	70	0.7441
Tissue	$134 \times 98 \times 72$	132	50	90	0.8536
Gamepad	$154 \times 104 \times 56$	262	50	80	—
Steamed cake	$102 \times 60 \times 44$	27	30	100	0.9962
Towel	$140 \times 72 \times 45$	31	40	100	0.9648
Sponge	$200 \times 200 \times 15$	10	30	90	0.5114
Earpick	$\varphi 1.8 \times 75$	4	15	100	—
Toothpick	$\varphi 1.7 \times 62$	<1	10	90	—
Business card	$90 \times 56 \times 0.4$	1	15	100	0.9998

Table 7: Comparison of grasping results.

Reference	Min size (mm)	Max size (mm)
Our gripper	1.7	200
[16]	2	170
[17]	10	100
[18]	24	100
[10]	24	100

the success rate of grasping does not necessarily decrease. For example, although the stability coefficient w of the sponge is small, its weight is only 10 g, so the success rate can reach 100%. The success rate of the barrel surface with a large weight, small stability coefficient, and smooth surface is the lowest, only 70%. The success rate of small weight objects with a large stability coefficient is above 90%.

5.3. Comparison Analysis. The grasping results are compared with the existing references, and the comparison table is shown in Table 7.

It can be seen from Table 7 that there is a great improvement in the grasp size. References [11–15] are used to grasp specific objects, and the grasping range of [10, 16–18] is not as large as the grasping range designed in our study.

6. Conclusion and Future Work

In this paper, a new error term of the cost function is applied to DWA to improve the mobile robot navigation performance. It can make the robot travel along the global path as much as possible, reducing unnecessary running paths in the process of movement and improving the running efficiency. Additionally, a kind of pneumatic soft gripper for mobile robotic systems with automatically adjustable finger spacing is proposed. The gripper is mainly composed of four pneumatic soft fingers, a linear motor, and a connecting bracket. The fingertips of the gripper are designed to be pointed and flat in shape, and the purpose of this design is to achieve small object grasping. The free control of the distance between fingers is realized through the slide rail controlled by the stepping motor to realize the grasping strategy from small to large. In addition, the grasping stability coefficient of the grasping objects is modelled and calculated. The work of a single finger mainly includes the following: (1) In terms of the fabrication technology, the soft finger is printed via a 3D printer, which has a printing accuracy of 0.02 mm, and can print rubber-like materials with different Shore hardnesses. This printer provides a convenient and quick finger fabrication method for the experiment and speeds up the experimental progress. (2) With respect to the finger bending angle analysis, nonlinear finite element analysis is carried out by using the finite element analysis software ABAQUS, and the relationship between the finger bending and air pressure is calculated. The relationship between the bending angle and the air pressure and the relationship between the bending angle and the Shore hardness are almost the same in the actual experiment and simulation. (3) In the fingertip force test, it is found that the smaller the Shore hardness is, the greater the fingertip force is. Combined with all the experimental results, the finger assembly with a Shore hardness of 30 was selected to carry out the grasp experiment. Finally, through a variety of different shapes and weights of the object used in the grasp experiment, the advantages of the gripper designed in this paper for grasping small to large objects are verified.

Currently, the fingertip force of the fingers studied in this paper is small, so it is difficult to grasp heavy objects. Under an air pressure of approximately 50 kPa, the pneumatic finger exhibits great bending, and it is difficult for the finger surface to have a large area contact with objects with relatively flat surfaces. Most of the objects are grasped by the fingertip, which plays a major role, without spreading the force evenly to the whole finger. In future research, we will further improve the finger's grasping performance for grasping heavy objects. We also need to improve the freedom of the finger movement, such as increasing the function of rotating fingers, increasing the multiple directions of movement, and other functions. Thus, most of the objects can be grasped in the manner of an optimal grasping position. Finally, the success rate of grasping is improved.

Data Availability

The data in this paper are obtained through experiments and references. Data are also available from the corresponding author via e-mail (yqchen@cuhk.edu.cn).

Conflicts of Interest

The authors declare that they have no conflicts of interest.

Acknowledgments

This work was partially supported by the National Natural Science Foundation of China (U1613216) and Shenzhen Fundamental Research grant (JCYJ20180508162406177) from the Chinese University of Hong Kong, Shenzhen. This work was also partially supported by funding from Shenzhen Institute of Artificial Intelligence and Robotics for Society and the Zhejiang Lab's International Talent Fund for Young Professionals.

References

[1] M.-S. Kang, C. Ihm, J. Lee, E.-H. Choi, and S. K. Lee, "A study on object recognition for safe operation of hospital logistics robot based on IoT," *The Journal of the Institute of Internet Broadcasting and Communication*, vol. 17, no. 2, pp. 141–146, 2017.

[2] F. Lee and S. Ivanov, "Understanding the robotic restaurant experience: a multiple case study," 2020.

[3] F. Coelho, S. Relvas, and A. P. F. D. Barbosa-Póvoa, "Simulation of an order picking system in a manufacturing supermarket using collaborative robots," in *Proceedings of the 32nd Conference on Modelling and Simulation*, pp. 83–88, Wilhelmshaven, Germany, May 2018.

[4] A. Lourenço, F. Marques, R. Mendonça et al., "On the design of the ROBO-PARTNER intra-factory logistics autonomous robot," in *Proceedings of the 2016 IEEE International*

Conference on Systems, Man, and Cybernetics (SMC), pp. 2647–2652, IEEE, Budapest, Hungary, October 2016.

[5] W. J. Lee, S. I. Kwag, and Y. D. Ko, "Optimal capacity and operation design of a robot logistics system for the hotel industry," *Tourism Management*, vol. 76, Article ID 103971, 2020.

[6] A. Zeng, K. T. Yu, S. Song et al., "Multi-view self-supervised deep learning for 6D pose estimation in the amazon picking challenge," in *Proceedings of the 2017 IEEE international Conference on Robotics and Automation (ICRA)*, pp. 1386–1383, IEEE, Singapore, May 2017.

[7] L. Zhang, L. Liu, and S. Zhang, "Design, implementation, and validation of robust fractional-order PD controller for wheeled mobile robot trajectory tracking," *Complexity*, vol. 2020, Article ID 9523549, 12 pages, 2020.

[8] C. Rösmann, F. Hoffmann, and T. Bertram, "Integrated online trajectory planning and optimization in distinctive topologies," *Robotics and Autonomous Systems*, vol. 88, pp. 142–153, 2017.

[9] D. Fox, W. Burgard, and S. Thrun, "The dynamic window approach to collision avoidance," *IEEE Robotics & Automation Magazine*, vol. 4, no. 1, pp. 23–33, 1997.

[10] Z. Wang, Y. Torigoe, and S. Hirai, "A prestressed soft gripper: design, modeling, fabrication, and tests for food handling," *IEEE Robotics and Automation Letters*, vol. 2, no. 4, pp. 1909–1916, 2017.

[11] Z. Wang, D. S. Chathuranga, and S. Hirai, "3D printed soft gripper for automatic lunch box packing," in *Proceedings of the 2016 IEEE International Conference on Robotics and Biomimetics (ROBIO)*, pp. 503–508, IEEE, Qingdao, China, December 2016.

[12] Z. Wang and S. Hirai, "A 3D printed soft gripper integrated with curvature sensor for studying soft grasping," in *Proceedings of the 2016 IEEE/SICE International Symposium on System Integration (SII)*, pp. 629–633, IEEE, Sapporo, Japan, December 2016.

[13] Z. Wang and S. Hirai, "Soft gripper dynamics using a line-segment model with an optimization-based parameter identification method," *IEEE Robotics and Automation Letters*, vol. 2, no. 2, pp. 624–631, 2017.

[14] Z. Wang and S. Hirai, "Geometry and material optimization of a soft pneumatic gripper for handling deformable object," in *Proceedings of the 2018 IEEE international conference on robotics and biomimetics (ROBIO)*, pp. 612–617, IEEE, Kuala Lumpur, Malaysia, December 2018.

[15] Y. Kuriyama, Y. Okino, Z. Wang et al., "A wrapping gripper for packaging chopped and granular food materials," in *Proceedings of the 2019 2nd IEEE international conference on soft robotics (RoboSoft)*, pp. 114–119, IEEE, Seoul, South Korea, April 2019.

[16] Y. Hao, Z. Gong, Z. Xie et al., "A soft bionic gripper with variable effective length," *Journal of Bionic Engineering*, vol. 15, no. 2, pp. 220–235, 2018.

[17] G. Zhong, Y. Hou, and W. Dou, "A soft pneumatic dexterous gripper with convertible grasping modes," *International Journal of Mechanical Sciences*, vol. 153-154, pp. 445–456, 2019.

[18] K. Batsuren and D. Yun, "Soft robotic gripper with chambered fingers for performing in-hand manipulation," *Applied Sciences*, vol. 9, no. 15, p. 2967, 2019.

[19] H. Fu and W. Zhang, "The development of a soft robot hand with pin-array structure," *Applied Sciences*, vol. 9, no. 5, p. 1011, 2019.

[20] C. K. Yoon, "Advances in biomimetic stimuli responsive soft grippers," *Nano Convergence*, vol. 6, no. 1, pp. 1–14, 2019.

[21] O. A. Abubakr, M. A. K. Jaradat, and M. A. Hafez, "A reduced cascaded fuzzy logic controller for dynamic window weights optimization," *in Proceedings of the 2018 11th International Symposium on Mechatronics and its Applications (ISMA),* IEEE, Sharjah, UAE, March 2018.

[22] M. Missura and M. Bennewitz, "Predictive collision avoidance for the dynamic window approach," in *Proceedings of the 2019 international conference on robotics and automation (ICRA)*, pp. 8620–8626, IEEE, Montreal, Canada, May 2019.

[23] H. Su, Y. Hu, H. R. Karimi et al., "Improved recurrent neural network-based manipulator control with remote center of motion constraints: experimental results," *Neural Networks*, vol. 131, pp. 291–299, 2020.

[24] F. H. Ajeil, I. K. Ibraheem, A. T. Azar, and A. J. Humaidi, "Grid-based mobile robot path planning using aging-based ant colony optimization algorithm in static and dynamic environments," *Sensors*, vol. 20, no. 7, p. 1880, 2020.

[25] H. Su, W. Qi, C. Yang, J. Sandoval, G. Ferrigno, and E. D. Momi, "Deep neural network approach in robot tool dynamics identification for bilateral teleoperation," *IEEE Robotics and Automation Letters*, vol. 5, no. 2, pp. 2943–2949, 2020.

[26] I. M. Meththananda, S. Parker, M. P. Patel, and M. Braden, "The relationship between Shore hardness of elastomeric dental materials and Young's modulus," *Dental Materials*, vol. 25, no. 8, pp. 956–959, 2009.

[27] J. Gafford, Y. Ding, A. Harris et al., "Shape deposition manufacturing of a soft, atraumatic, and deployable surgical grasper," *Journal of Mechanisms and Robotics*, vol. 7, no. 2, 2015.

[28] K.-J. Cho, J.-S. Koh, S. Kim, Y. Hong, and S.-H. Ahn, "Review of manufacturing processes for soft biomimetic robots," *International Journal of Precision Engineering and Manufacturing*, vol. 10, no. 3, pp. 171–181, 2009.

[29] Y. Xia and G. M. Whitesides, "Soft lithography," *Annual Review of Materials Science*, vol. 28, no. 1, pp. 153–184, 1998.

[30] A. D. Marchese, R. K. Katzschmann, and D. Rus, "A recipe for soft fluidic elastomer robots," *Soft Robotics*, vol. 2, no. 1, pp. 7–25, 2015.

[31] B. S. Homberg, R. K. Katzschmann, M. R. Dogar et al., "Haptic identification of objects using a modular soft robotic gripper," in *Proceedings of the 2015 IEEE/RSJ International Conference on Intelligent Robots and Systems (IROS)*, pp. 1698–1705, IEEE, Hamburg, Germany, September 2015.

[32] R. K. Katzschmann, A. D. Marchese, and D. Rus, "Hydraulic autonomous soft robotic fish for 3D swimming," *Experimental Robotics*, pp. 405–420, Springer, Berlin, Germany, 2016.

[33] J. T. Muth, D. M. Vogt, R. L. Truby et al., "Embedded 3D printing of strain sensors within highly stretchable elastomers," *Advanced Materials*, vol. 26, no. 36, pp. 6307–6312, 2014.

[34] H. Su, C. Yang, and G. Ferrigno, "Improved human-robot collaborative control of redundant robot for teleoperated minimally invasive surgery," *IEEE Robotics and Automation Letters*, vol. 4, no. 2, pp. 1447–1453, 2019.

[35] W. Qi, H. Su, and A. Aliverti, "A smartphone-based adaptive recognition and real-time monitoring system for human activities," *IEEE Transactions on Human-Machine Systems*, vol. 50, no. 5, pp. 414–423, 2020.

[36] C. H. Ko and J. S. Chen, "Optimal grasping manipulation for multifingered robots using semismooth Newton method,"

Mathematical Problems in Engineering, vol. 2013, Article ID 681710, 9 pages, 2013.

[37] Z. Li and S. S. Sastry, "Task-oriented optimal grasping by multifingered robot hands," *IEEE Journal on Robotics and Automation*, vol. 4, no. 1, pp. 32–44, 1988.

[38] C. Xiong and Y. Xiong, "Stability index and contact configuration planning for multifingered grasp," *Journal of Robotic Systems*, vol. 15, no. 4, pp. 183–190, 1998.